Photoinduced Charge Separation of Methylphenothiazine in Vanadium- and Titanium-Containing AlPO-5 and AlPO-11

Zhixiang Chang, Ranjit Koodali, R. M. Krishna, and Larry Kevan*

Department of Chemistry, University of Houston, Houston, Texas 77024-5641

Received: February 9, 2000; In Final Form: April 13, 2000

The photoinduced charge separation of methylphenothiazine in aluminophosphate type 5 and 11 (AlPO-5 and AlPO-11) containing Ti(TAPO-5, 11) and V(VAPO-5,11) is studied with near UV irradiation at room temperature. Methylphenothiazine cation radicals (PC_1^+) are produced in MAPO-5, 11(M = Ti^{4+} and V^{5+}) molecular sieves, and characterized by electron spin resonance and diffuse reflectance UV−vis spectroscopy. MAPO-5,11 molecular sieves are shown to be effective heterogeneous hosts to accomplish long-lived photoinduced electron transfer of methylphenothiazine (PC_1) molecules at room temperature. A series of MAPO-5,11 samples are synthesized that increase the PC_1 photoionization efficiency in comparison with AlPO-5,11. The photoionization efficiency increases in the order AlPO-11 < AlPO-5 < TAPO-11 < TAPO-5 < VAPO-11 < VAPO-5. It is found that the photochemistry in MAPO-5,11 molecular sieves depends on the type of transition metal ion and the AlPO pore size.

Introduction

In the photoredox reaction

$$A + D \xrightarrow{h\nu} A^- + D^+ \qquad (1)$$

a large fraction of the incident light energy may be initially converted into chemical energy. The practical application of such a system is hampered by the fact that back electron transfer often occurs rapidly. Thereby, the chemical potential available in the radical ions A^- and D^+ is degraded thermally. Current research is oriented toward the design of efficient photoredox systems that can inhibit back electron transfer and lead to relatively stable charge separation between the electron donor and the electron acceptor.[1−6]

The back electron transfer rate is often retarded in heterogeneous systems, compared to homogeneous solutions. The photoionizaton efficiency in organic assembles is often higher than that in homogeneous solution, but the photoinduced radicals are not typically stable at room temperature. In some cases, the polarity and solubility of a photodonor in vesicular and micellar solutions [7,8] limit the photoyield in organic assemblies. However, photoinduced charge separation in porous inorganic materials such as zeolites[9−12] and silica gel[13,14] have shown that these materials provide steric and electrostatic microenvironments to retard back electron transfer and increase the lifetime of photoinduced radical ions.

Methylphenothiazine (PC_1) is an efficient electron donor molecule. It can be easily photooxidized to form the methylphenothiazine cation radical (PC_1^+), which can be characterized by electron spin resonance (ESR) and optical spectroscopic techniques.[13] It can also be photooxidized by near UV irradiation. Flash photolysis has been used to study the photooxidation of PC_1 in micelles with metal ions as electron acceptors at micelle surfaces, and it was shown that the photooxidation, or photoionization, is a monophotonic process.[15,16] The conversion of phenothiazine and methylphenothiazine into phenothiazine and methylphenothiazine cations was observed. Recent ESR and optical adsorption results of N-alkylphenothiazine derivatives in silica gels,[13] layered zirconium phosphate,[17] and molecular sieves[12] demonstrated that long-lived charge separation can be achieved at room temperature.

Microporous aluminophosphate (AlPO-*n*) molecular sieves seem amenable to framework substitution by a variety of transition metal ions[12,18] that can act as redox sites and decrease back electron transfer. Transition metal ion containing AlPO-*n* materials look promising as photoredox systems for long-lived charge separation.

In this research, a series of Ti- and V-containing AlPO-5,11 materials (TAPO-5,11 and VAPO-5,11) with different Ti and V content have been synthesized and used as heterogeneous hosts for photoinduced electron transfer from PC_1. The photoinduced PC_1^+ cation is characterized by ESR and diffuse reflectance (DR) UV−vis spectroscopy. It is clear that V^{5+} is an electron acceptor because V^{4+} can be observed by ESR. The PC_1^+ photoyield and its stability in these materials, measured by ESR, depends on the AlPO pore size and the type of transition metal ion. The PC_1^+ photoyield increases in the order AlPO-11 < AlPO-5 < TAPO-11 < TAPO-5 < VAPO-11 < VAPO-5, indicating that the framework modified by incorporating Ti^{4+} or V^{5+} into AlPO-5,11 enhances the electron-accepting ability of the AlPO-5,11 framework. PC_1^+radicals are more stable at room temperature in TAPO-11, VAPO-11, and VAPO-5, compared to TAPO-5.

Experimental Section

Materials. The following chemicals were used without further purification: orthophosphoric acid (Malliincrodt, 85%), aluminum isopropoxide (Acros, 98+%), pseudoboehmite (Catapal B, Vista Chemical Co.), triethylamine (Pr_3N, Fisher, 99%), tetrapropylammonium hydroxide (TPAOH, Alfa), di-*n*-propylamine (Pr_2NH, Alfa, 99%) and vanadyl sulfate hydrate (Alfa, 99%). The source of Ti was titanium isopropoxide (Aldrich) for TAPO-5 and titanium butoxide (Alfa) for TAPO-11. Anatase TiO_2, with a 50 Å particle diameter, was obtained from Aldrich.

10.1021/jp000505b CCC: $19.00
Published on Web 05/19/2000

Deionized water was used throughout the syntheses. A Teflon lined 100 cm^3 stainless steel reactor was used for crystallization.

Synthesis of TAPO-5, VAPO-5, and AlPO-5. TAPO-5 was prepared hydrothermally using TPAOH as the organic template, following an earlier procedure.[19] The synthesis of VAPO-5 was performed by a modified method for VAPO-5.[20] First, 23.1 g of orthophosphoric acid was mixed with 68.3 g of water. Then, to the solution was slowly added 11.1 g of pseudoboehmite. After about 2 h of stirring, to this slurry was added 17.9 g of TEA dropwise, and the gel was stirred for 2 h. Finally, to the above gel was added dropwise the required amount of vanadyl sulfate dissolved in 10 g of water, and the gel was stirred for further 2 h. The molar composition of the final gel was 1 P_2O_5:1 Al_2O_3:(0.005∼0.12) TiO_2:0.8 TPAOH:40 H_2O. The resulting gel was crystallized at 573 K for 16 h. After crystallization, the product was separated from the mother liquid, washed with water, and dried at 373 K overnight. To remove the organic template, the as-synthesized material was calcined in flowing nitrogen while the temperature was raised slowly to 823 K and then in flowing oxygen for 10 h. These calcined samples are termed TAPO-5(*n*) and VAPO-5(*n*), where *n* indicates the P/Ti ratio or P/V ratio. The calcined material was cooled to room temperature and kept in a desiccator until impregnation with PC_1.

Synthesis of TAPO-11, VAPO-11, and AlPO-11. Synthesis of TAPO-11, VAPO-11, and AlPO-11 was achieved following a literature procedure[21,22] with some modification. Pretreatment of the final gel for synthesis of AlPO-11 at 363 K can prevent the production of condensed phase impurities. Without such a treatment, condensed phase impurities are often observed. This difference may be related to the formation of a metavariscite/variscite structure in the gel during the 363 K pretreatment.[22] On the basis of preliminary experiments, the following molar compositions were used for the crystallization of AlPO-11 materials: 1 P_2O_5:1 Al_2O_3:(0.01∼0.15) TiO_2:0.90 Pr_2NH:57 H_2O for TAPO-11 and 1 P_2O_5:1 Al_2O_3:(0.00∼0.12) V_2O_5:0.90 Pr_2NH:57 H_2O for VAPO-11.

The synthetic procedure for TAPO-5 was as follows. First, 40.9 g of aluminum isopropoxide was soaked with a required amount of water and stirred for 4 h. The required amount of Ti butoxide was dissolved in a mixture of water, hydrogen peroxide and orthophosphoric acid and added dropwise into the above gel with stirring. After 2 h of stirring, to the gel was slowly added 9.2 g of Pr_2NH, and the gel was stirred for another 2 h. The final gel was transferred to a Teflon-lined autoclave, preheated at 363 K for 24 h, and further heated at 573 K for another 24 h.

In a typical preparation of VAPO-11 and AlPO-11, 40.9 g of orthophosphoric acid was first diluted with 89.2 g of water. To this solution was very slowly added aluminum isopropoxide. After 4 h of stirring, the required amount of vanadyl sulfate dissolved in 10.0 g of water was added dropwise to the above gel under stirring and was stirred for an additional 1 h. Finally, to the resultant was slowly added 9.2 g of Pr_2NH, which was stirred for another 2 h. The crystallization was done under the same conditions as those for TAPO-11. The as-synthesized samples were dried and calcined as described above. These calcined samples are termed TAPO-11(*n*) and VAPO-11(*n*), where *n* indicates the P/Ti or P/V ratio.

Sample Preparation for Photoirradiation and Measurement. Methylphenothiazine (Aldrich) was incorporated into AlPO-5,11; TAPO-5,11; and VAPO-5,11 by impregnation. For impregnation, 0.5 g of the AlPO material was immersed in 2 mL of 10^{-2} M PC_1−C_6H_6 solution overnight, and the solvent was then removed by flowing nitrogen through the solution for about 50 min. The loading of PC_1 in AlPO-5,11 and VAPO-5,11 was 40 μmol/g. For ESR measurements, the sample powder was filled into 2 mm i.d. × 3 mm o.d. Suprasil quartz tubes to about 20 mm in height. The tube was connected to a vacuum line and evacuated to about 1×10^{-4} Torr. The samples were then sealed in the tube under vacuum. For DR UV−vis measurements, the sample powder was put into a cylindrical quartz sample cell (19 mm diameter × 1 mm path length) which was evacuated to about 10^{-4} Torr and sealed. All of the samples were handled in the dark to minimize exposure to visible light.

X-ray powder diffraction patterns were recorded on a Philips PW1840 diffractometer using Cu Kα radiation (40 kV, 25 mA) with a 0.025 step size and 1 s step time over range $4° < 2\theta < 50°$ for AlPO-5 samples and $4° < 2\theta < 40°$ for AlPO-11 samples. The samples were prepared as thin layers on aluminum slides. The elemental composition of the samples was analyzed by a JEOL JXA-8600 electron microprobe with a beam diameter of 20 nm. The resolution is 2.5 eV. Five or more randomly selected spots on the samples were averaged. The ESR spectra were recorded at room temperature at X-band frequency using a Bruker ESP 300 spectrometer with 100 kHz field modulation and microwave power sufficiently low to avoid saturation. The photoproduced PC_1^+ radical yields were determined by subtracting the ESR intensity of any dark reaction from that of photoirradiated samples by double integration of the ESR spectra using the ESP 300 software. The DR UV−vis spectra were recorded before and after different times of photoirradiation at room temperature using a Perkin−Elmer model 330 spectrophotometer with an integrating sphere accessory.

The evacuated PC_1-AlPO-5,11; PC_1-TAPO-5,11; and PC_1-VAPO-5,11 samples were irradiated with a 300 W Cermax xenon lamp (ILC-LX 300 UV) at room temperature. The light was passed through a 10 cm water filter and a Corning No. 7-51 glass filter, which passes light of wavelength longer than 320 nm. Every sample was irradiated in a quartz dewar that was rotated at 4 rpm to ensure even irradiation of the samples. The photoproduced PC_1^+ radical was identified by ESR and UV−vis spectroscopy.

Results

AlPO-5,11, TAPO-5,11 and VAPO-5,11 Samples. AlPO-5 and AlPO-11 are two novel microporous AlPO molecular sieves. The AlPO-5 molecular sieve is composed of 4-ring, 6-ring, and 12-ring straight channels, which are interconnected by 6-ring windows. The main channel opening of AlPO-5 is 7.3 × 7.3 Å. The removal of a pair of opposing 4-rings in AlPO-5 converts the 12-ring to a 10-ring and generates AlPO-11.[23] The main channel opening of AlPO-11 is 7.0 × 4.1 Å. The XRD patterns of as-synthesized AlPO-5,11 and MAPO-5,11 (M = Ti and V) are presented in Figures 1 and 2. From the XRD spectra, it was found that all the samples have good crystallinity. Because the XRD patterns of MAPO-5 and MAPO-11 are nearly the same as those of AlPO-5 and AlPO-11, respectively, it is clear that MAPO-5 and MAPO-11 samples possess the same framework topology as AlPO-5 and AlPO-11.

The DR UV−vis spectra of TAPO-5,11 are shown in Figures 3 and 4. Compared with bulk anatase (TiO_2 particles of 50 Å diameter), the absorption edges of all TAPO-5,11 samples are blue-shifted by more than 50 nm. Tetrahedral framework Ti was observed to exist in TS-1 as open $(SiO_3)_3$ TiOH and closed (SiO_4) Ti species with absorption bands at 220 and 270 nm, respectively.[19] The DR UV−vis spectra of these TAPO-5,11 samples with low Ti content (Si/Ti > 50) show a maximum at

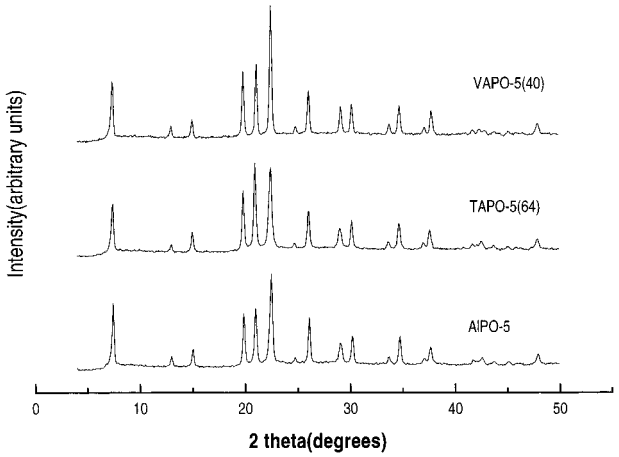

Figure 1. XRD patterns of as-synthesized VAPO-5, TAPO-5, and AlPO-5.

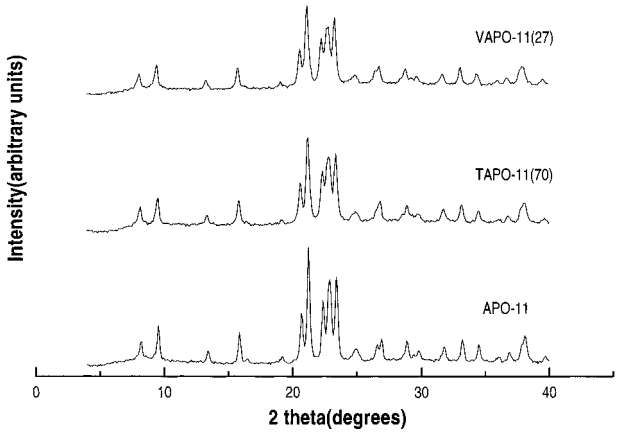

Figure 2. XRD patterns of as-synthesized VAPO-11, TAPO-11, and AlPO-11.

230−270 nm that can be assigned to ligand-to-metal charge-transfer transitions between oxygen and tetracoordinated Ti^{4+} ions,[24,25] suggesting that the two kinds of isolated tetrahedral Ti species are probably present in these materials. This indicates that Ti^{4+} is incorporated into the framework of AlPO-5,11.[19,26−28] The DR UV−vis spectra of TAPO-5,11 samples show no significant adsorption at 300−350 nm, indicating that a segregated crystalline TiO_2 phase-like anatase is absent in TAPO-5,11 samples. But TAPO-5,11 samples of higher Ti concentration show a broad, red-shifted absorption band at 200−350 nm comparable to TAPO-5,11 with lower Ti contents. This indicates that the Ti^{4+} ions in TAPO-5,11 samples of higher Ti content are present partly in tetrahedral framework positions and partly as TiO_2 particles.

The DR spectra in the UV−vis region were obtained to characterize the structure of V in VAPO-5,11. The charge transfer transition energy is strongly influenced by the number of ligands on the central ion which gives information on the coordination of V.[29,30] As the number of ligands to V decreases from 6 to 4, the absorption bands shift to shorter wavelength, and tetrahedrally coordinated V^{5+} shows absorption below 350 nm. The charge-transfer band at 450 nm is the most characteristic of the DR spectrum of V_2O_5 (Figure 5A) and has been attributed to charge transfer to a delocalized acceptor site, such as those on VO_6 chains. The presence of a band at 270−300 nm is indicative of isolated tetrahedral V^{5+} sites.[20]

The DR UV−vis spectra of calcined VAPO-11 samples with different V contents are shown in Figure 5. The VAPO-11 samples of lower V content (P/V > 27) show absorption near

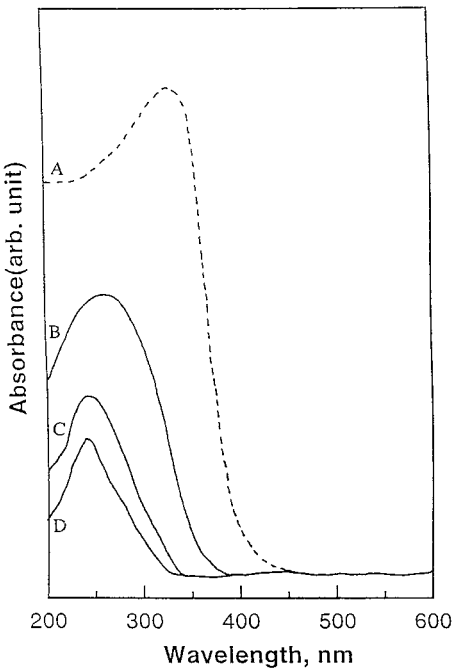

Figure 3. Diffuse reflectance UV−vis spectra of (A) anatase with 50 Å particle diameter, (B) TAPO-5 (25), (C) TAPO-5 (64), and (D) TAPO-5 (106).

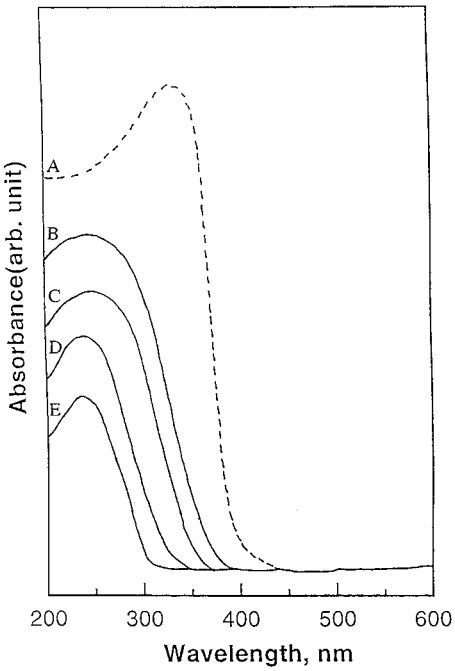

Figure 4. Diffuse reflectance UV−vis spectra of (A) anatase with 50 Å particle diameter, (B) TAPO-11 (25), (C) TAPO-11 (50), (D) TAPO-11 (70), and (E) TAPO-11 (99).

280 nm, which indicates that V has tetrahedral coordination. The absence of any absorptions above 550 nm in calcined samples demonstrates that little V^{4+} is present, in accord with the ESR results. For as-synthesized VAPO-11 samples, a charge-transfer absorption band near 280 nm is observed, together with an absorption band extending over 500−800 nm due to d−d transitions of V^{4+}.[31] V appears to have tetrahedral coordination in both as-synthesized and calcined VAPO-11. This indicates that V is incorporated into a tetrahedral position of the AlPO-11 framework.[20,32−35] VAPO-11 with higher V content shows a maximum near 300 nm and a shoulder near 450 nm, suggesting that some vanadium−oxygen polymeric species is

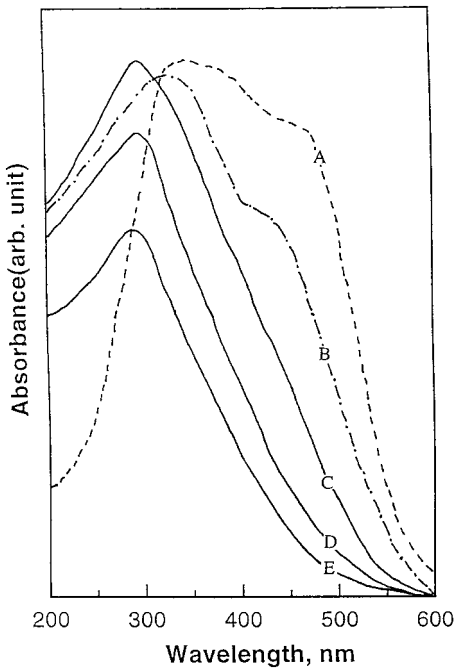

Figure 5. Diffuse reflectance UV−vis spectra of (A) V_2O_5, (B) VAPO-11 (20), (C) VAPO− 11(27), (D) VAPO-11 (66), and (E) VAPO-11 (112).

present. So V^{5+} ions are present partly in tetrahedral coordination in the framework and partly as V_2O_5.

Blasco[20] et al. studied the preparation, characterization and catalytic properties of VAPO-5, and proposed that isolated, tetrahedral V^{5+} species in the framework were the active and selective sites for oxydehydrogenation of propane. The DR UV−vis spectra of calcined VAPO-5 show an absorption maximum near 290 nm, indicating that V is incorporated into the AlPO-5 framework.[32,36] VAPO-5 with the higher V concentration of P/V $\leq$ 40 is not thermally stable, although the as-synthesized VAPO-5 has good crystallinity. Its structure is completely destroyed if it is calcined at 573 K.

PC_1^+ Analysis by ESR and DR UV−Vis Spectroscopy. The ESR spectra from photoinduced PC_1^+ in MAPO-5,11 and AlPO-5,11samples after 180 min of photoirradiation with $\lambda >$ 320 nm at room temperature are shown in Figure 6. The samples show a strong ESR signal of PC_1^+ at $g = 2006$ with incompletely resolved hyperfine.[14] The AlPO-5,11 and MAPO-5,11 samples without PC_1 give no ESR signals after irradiation. The DR UV−vis spectra of PC_1-TAPO-5(64) before and after irradiation at room temperature are shown in Figure 7. The DR spectra show a strong absorption in the UV region, which is assigned to PC_1 trapped in TAPO-5. After different UV irradiation times, the absorption spectrum in the visible range is the same as that for PC_1^+ cation radical in liquids, micelles, silica gels, layered materials, and zeolites.[11,37−39] A similar behavior is observed for all of the MAPO-5,11 samples. This shows that stable PC_1^+ radicals are produced by > 320 nm irradiation at room temperature and confirm the photoionization of PC_1 into PC_1^+ in TAPO-5(64).

Photoyields in TAPO-5,11. Figure 8 shows the increase in the ESR intensities for MAPO-5,11 and AlPO-5,11 samples impregnated with PC_1 with irradiation time. The ESR signal increases rapidly during the first 30 min and reaches a plateau after about 180 min. An irradiation time of 180 min was selected for comparative photoyield and stability studies. The low loadings(0.01 M) of PC_1 correspond to optimal photoyields. The 0.01 M loadings cover about 5% of the surface area of the

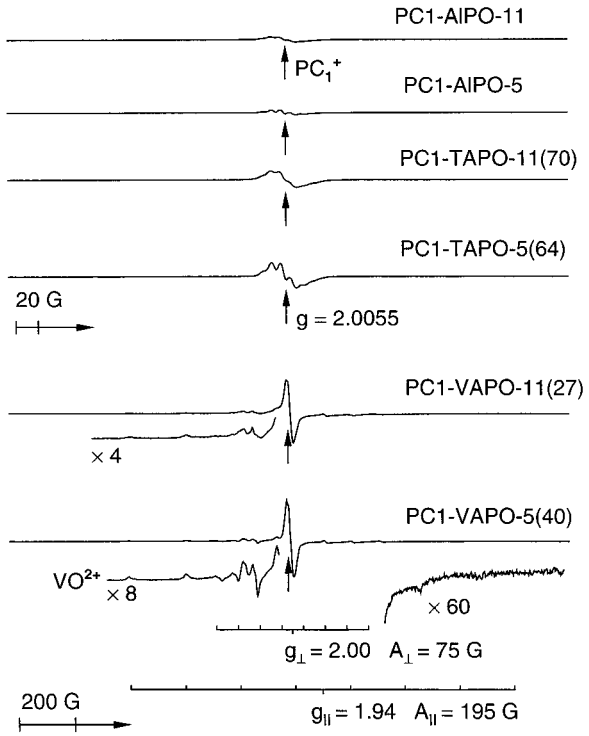

Figure 6. ESR spectra of photoinduced PC_1^+ cation radical in AlPO-5,11 and MAPO-5,11 (M = Ti^{4+}, V^{5+}) after 180 min irradiation with >320 nm light at room temperature.

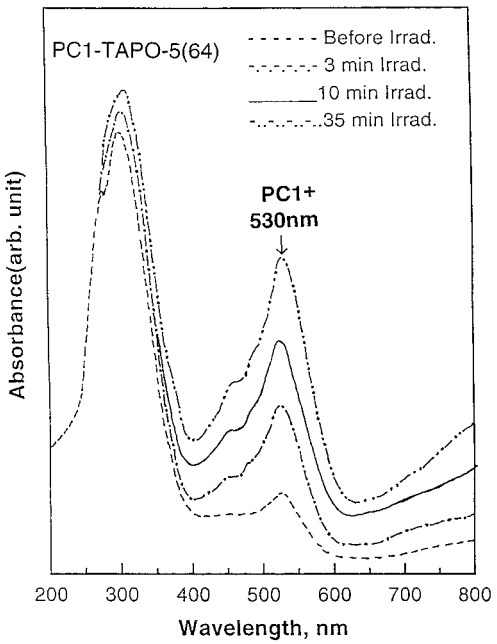

Figure 7. Diffuse reflectance UV−vis spectra of photoinduced PC_1^+ radical in TAPO-5 before and after different irradiation times with >320 nm light at room temperature.

MAPO-5,11 and AlPO-5,11 samples. The PC_1-TAPO-5,11 samples prepared by impregnation are light pink in color before irradiation and turn deep pink after irradiation, which is characteristic of the PC_1^+ cation.[14] This confirms the photoionization of PC_1 into PC_1^+ cation radical in TAPO-5,11. PC_1-TAPO-5,11 samples give higher photoyields than PC_1-AlPO-5,11 and lower photoyields in comparison with PC_1-VAPO-5,11 as shown in Figure 9. The photoyields in TAPO-5,11 versus increasing Ti content in TAPO-5,11 are shown in Figures 10 and 11. The photoyield for TAPO-5 increases to a P/Ti ratio of

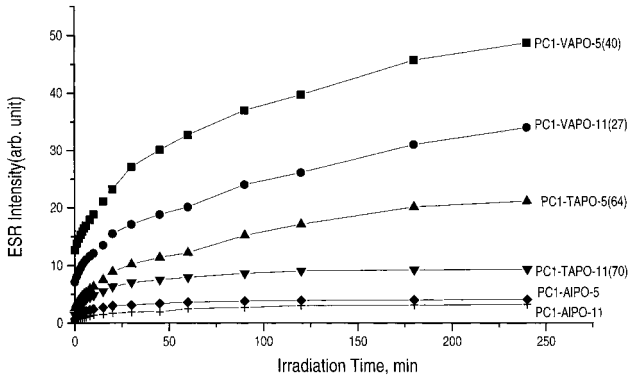

Figure 8. Increase of ESR intensities of PC_1^+ radical at room temperature versus >320 nm irradiation for AlPO-5,11 and MAPO-5,11(M = Ti^{4+}, V^{5+}) samples.

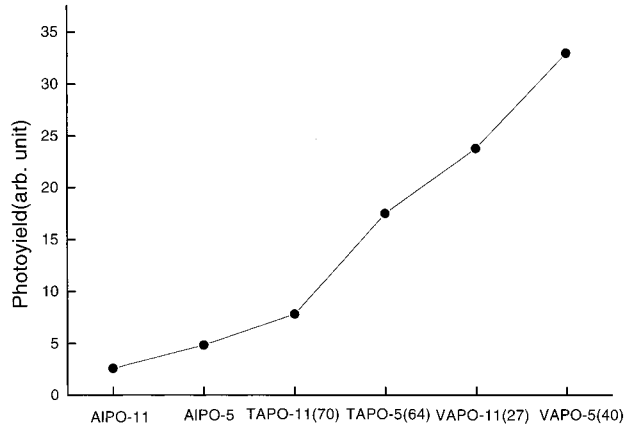

Figure 9. PC_1^+ photoyields in AlPO-5,11 and MAPO-5,11(M = Ti^{4+}, V^{5+}) samples after 180 min irradiation with >320 nm light at room temperature.

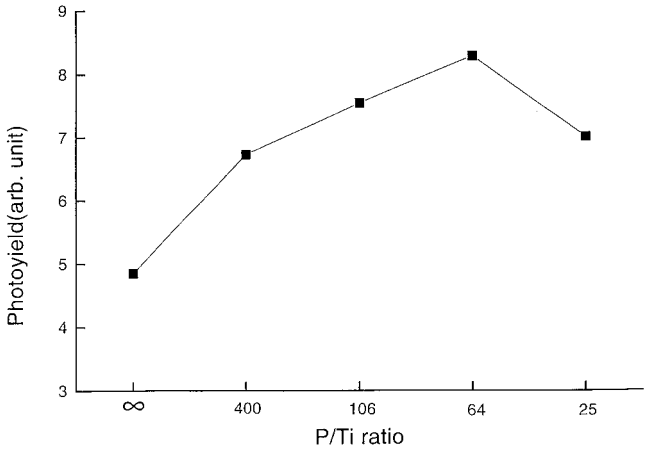

Figure 10. PC_1^+ photoyields in TAPO-5 samples versus Ti content after 180 min irradiation with >320 nm light at room temperature.

64, and then decreases for a P/Ti ratio of 25. The photoyield for TAPO-11 reaches a maximum at a P/Ti ratio of 70.

Photoyields in VAPO-5,11. Figure 9 shows that the PC_1^+ photoyield is greatest in VAPO-5,11 compared with AlPO-5,11 and TAPO-5,11. The photoyield in VAPO-5 increases with increasing V content as shown in Figure 12. The photoyield for VAPO-11 increases for a P/V ratio of 27 and then decreases for a P/V of 20 (Figure 13). The color of fresh, evacuated PC_1-VAPO-5,11 is pink before irradiation and turns dark brown after irradiation. VAPO-5,11 samples have a stronger dark reaction than TAPO-5,11 and AlPO-5,11. The variation in the ESR intensities of the photoinduced PC_1^+ signals measured at room

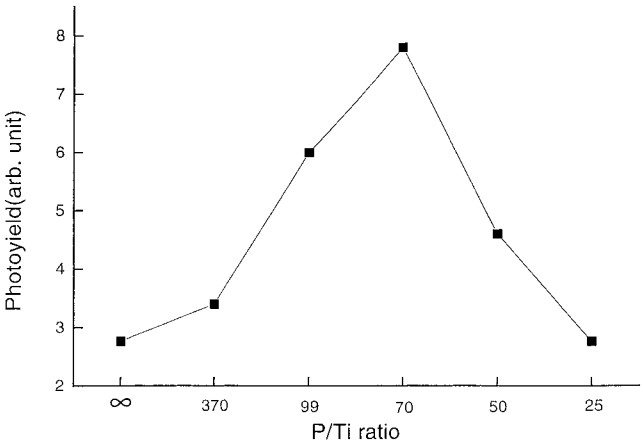

Figure 11. PC_1^+ photoyields in TAPO-11 samples versus Ti content after 180 min irradiation with >320 nm light at room temperature.

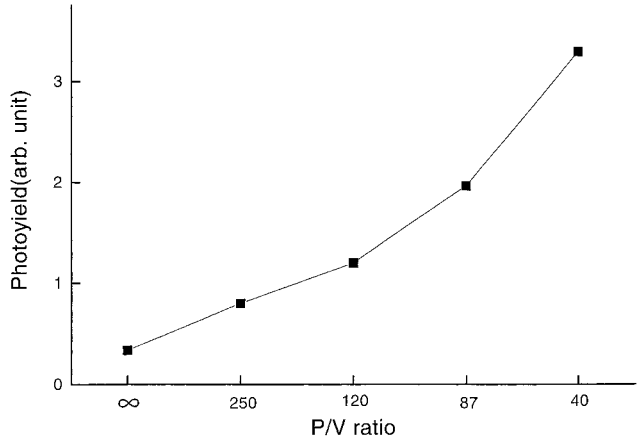

Figure 12. PC_1^+ photoyields in VAPO-5 samples versus V content after 180 min irradiation with >320 nm light at room temperature.

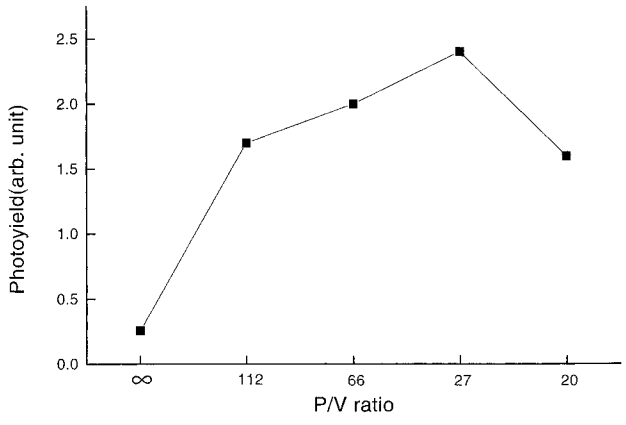

Figure 13. PC_1^+ photoyields in VAPO-11 samples versus V content after 180 min irradiation with >320 nm light at room temperature.

temperature versus decay time after >320 nm irradiation are shown in Figure 14. The PC_1^+ cation radicals in VAPO-5,11 and TAPO-11 are more stable than those in TAPO-5. Thus, the photoyield and stability of PC_1^+ cation radicals are affected by the pore size of AlPO molecular sieves and the type of transition metal ion.

Discussion

The ESR and DR UV−vis results clearly confirm the photooxidation of PC_1 molecules into PC_1^+ cation radicals in AlPO-5,11 and MAPO-5,11 samples by >320 nm irradiation

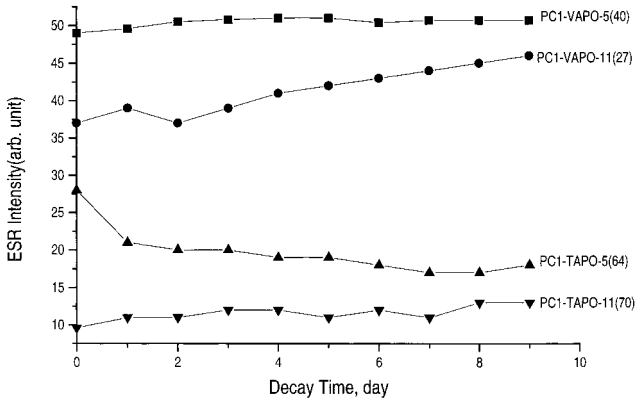

Figure 14. Decay of ESR intensities of PC_1^+ at room temperature for MAPO-5,11 ($M = Ti^{4+}$, V^{5+}) samples with time after 180 min room temperature irradiation with >320 nm light.

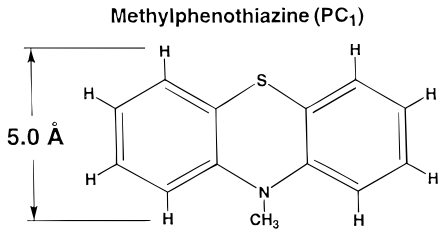

Figure 15. Methylphenothiazine structure.

at room temperature. Methylphenothiazine (PC_1) has the structure shown in Figure 15. The main channel opening of AlPO-5 is larger than the size of PC_1, so all PC_1 molecules penetrate into AlPO-5. However, only part of the PC_1 penetrates into the AlPO-11 channel because the main channel opening of AlPO-11 is smaller, based on thermal analysis data.[12] So the photoyield of PC_1−AlPO-5 is larger than that of PC_1-AlPO-11 (Figure 9). The photoyield in PC_1-TAPO-5,11 has a maximum with increasing Ti content, probably because some nonframework Ti oxide in TAPO-5,11 at high Ti content blocks the main channels and results in less PC_1 penetrating into the TAPO-5,11 samples. From the higher photoyield in TAPO-5,11 compared with AlPO-5,11, it is suggested that TAPO-5,11 is a better electron acceptor than AlPO-5,11 due to reduction of Ti^{4+} to Ti^{3+} in the framework. For catalytic oxidation reactions of some aromatics, alkanes, and alcohols in Ti-substituted molecular sieves such as TS-1,[40,41] these molecules are selectively adsorbed on Ti^{4+} sites.[42] Similarly, for photoionization of PC_1 in TAPO-5,11, it seems that PC_1 molecules are preferentially adsorbed on surface Ti^{4+} sites and that Ti^{4+} is reduced to Ti^{3+} resulting in a higher photoyield. One may expect to see an ESR signal of Ti^{3+} species generated by photoelectron transfer from PC_1, but that is not detected at 77 K probably due to overlap with the PC_1^+ ESR signal. Overall, it seems that Ti^{4+} in TAPO-5,11 modifies the framework to enhance PC_1 adsorption and act as a better electron acceptor site to increase the PC_1^+ photoyield. Compared with PC_1-TiMCM-41,[43] PC_1-TAPO-5 has a higher photoyield, and the PC_1^+ radical is much more stable at room temperature. This is probably because TAPO-5 has a much smaller main channel than TiMCM-41 which can limit the mobility of PC_1^+ radicals to minimize back electron transfer and increase the lifetime of the photoinduced PC_1^+ radicals.

Samples of VAPO-5,11 impregnated with PC_1 show a stronger ESR signal of PC_1^+ cation radical compared with PC_1-AlPO-5,11 and TAPO-5,11 samples. Most importantly, V^{4+} is observed by ESR after photoirradiation. This supports that V^{5+} ions in VAPO-5,11 do accept electrons from PC_1 to enhance the PC_1^+ photoyield. The ESR of V^{4+} can be clearly observed in contrast to the ESR of Ti^{3+} because the overall spectral width of V^{4+} is wider due to ^{51}V hyperfine so that it is observable on top of the PC_1^+ ESR spectrum. The ESR intensities of both V^{4+} and PC_1^+ radical increase with irradiation time. The increase of the PC_1^+ spin concentration in PC_1-VAPO-5,11 is the same as that of the V^{4+} spin concentration during less than 1 h irradiation clearly indicating that V^{5+} is an electron acceptor. But at longer irradiation time, the increase of the PC_1^+ spin concentration is smaller than that of the increase in V^{4+} spin concentration, probably because of secondary reactions of PC_1^+.[6,13]

The photoyield of PC_1-VAPO-11 increases as the V concentration increases to a P/V ratio of 27 as shown in Figure 3. The photoyield of PC_1-VAPO-11 for P/V = 20 decreases probably because nonframework V_2O_5 blocks the main channel and results in less PC_1 molecules penetrating VAPO-11. PC_1-VAPO-5 shows the highest photoyield among the PC_1-MAPO-5,11 samples because VAPO-5 has a larger main channel opening than VAPO-11, and the V^{5+} ion has a stronger electron-accepting ability than Ti^{4+}. PC_1-VAPO-11 samples show higher photoyields than PC_1-TAPO-5,11 samples. Figure 6 shows that the initial slopes increase in the order AlPO-11 (4.8×10^{-3} s^{-1}) < AlPO-5 (8.8×10^{-3} s^{-1}) < TAPO-11 (1.3×10^{-2} s^{-1}) < TAPO-5 (1.4×10^{-2} s^{-1}) < VAPO-11 (1.6×10^{-2} s^{-1}) < VAPO-5 (1.9×10^{-2} s^{-1}). This indicates that both Ti^{4+} and V^{5+} are good electron acceptors. It seems that V^{5+} sites in the VAPO-5,11 framework enhance the electron-accepting ability of the framework over that of Ti^{4+} sites in the framework.

The ESR line shapes of photoinduced PC_1^+ trapped in MAPO-5,11 are only partially resolved at room temperature (Figure 6). The spectral resolution and line width depend on the mobility of the radical.[14] Fast motion averages out dipolar interaction and reduces the ESR line width. From Figure 6, we deduce that PC_1^+ radicals have more mobility in MAPO-5 samples than in MAPO-11 samples because MAPO-5 has a larger main channel than MAPO-11. This causes the PC_1^+ radical to be less stable in TAPO-5 compared to TAPO-11. PC_1^+ is more stable in VAPO-5, probably because V^{4+} is stable and it is difficult for V^{4+} to transfer an electron back to PC_1^+.

Conclusions

TAPO-5,11 and VAPO-5,11 molecular sieves are found to be promising hosts for long-lived photoinduced charge separation of adsorbed PC_1. The photoyield and stability of the PC_1^+ cation radicals depend on the AlPO pore size and the type of transition metal ions. The PC_1^+ photoyield increases in the order AlPO-11 < AlPO-5 < TAPO-11 < TAPO-5 < VAPO-11 < VAPO-5. The PC_1^+ radical is more stable in VAPO-5,11 and TAPO-11 compared with TAPO-5. It is clear that V^{5+} is an electron acceptor during the photoirradiation of PC_1-VAPO-5,11 samples. It seems that the Ti^{4+} and V^{5+} sites in the MAPO-5,11 framework enhance the electron-accepting ability of the framework.

Acknowledgment. This research was supported by the Division of Chemical Sciences, Office of Basic Energy Sciences; Office of Energy Research, US Department of Energy; the Robert A. Welch Foundation; the Texas Advanced Research Program; and the Environmental Institute of Houston.

References and Notes

(1) Krueger, J. S.; Mayer, J. E.; Mallouk, T. E. *J. Am. Chem. Soc.* **1988**, *110*, 8232.

(2) Vermeulen, L. A.; Thompson, M. E. *Nature* **1992**, *358*, 656.

(3) Slama-Schwok, A.; Avnir, D.; Ottolenghi, M. *Photochem. Photobiol*. **1991**, *54*, 525.
(4) Buck, H. M.; Bloemhoff, W.; Oostrhoff, L. *Tetrahedron Lett*. **1960**, *9*, 5.
(5) Forbes, W. F.; Sullivan, P. D. *J Am. Chem. Soc*. **1966**, *88*, 2862.
(6) Shine, H. J.; Thompson, D. R.; Veneziani, C. *J. Heterocycl. Chem*. **1967**, *4*, 517.
(7) Kalyanasundaram, K. *Photochemistry in Microheterogeneous Systems*; Academic: New York, 1987; Chapters 4 and 6.
(8) Sung-Suh, H. M.; Kevan, L. *J. Phys. Chem. A*. **1997**, *101*, 1414.
(9) Kim, Y. I.; Mallouk, T. E. *J. Phys. Chem*. **1992**, *96*, 2879.
(10) Sankaraman, S.; Yoon, K. B.; Yake, T.; Kochi, *J Am. Chem. Soc*. **1991**, *113*, 1419.
(11) Krishna, R. M.; Prakash, A. M.; Kurshew, V.; Kevan, L. *Phys. Chem. Chem. Phys*. **1999**, *1*, 4119.
(12) Kurshev, V.; Prakash, A. M.; Krishna. R. M.; Kevan, L. *Microporous Mesoporous Mater*. **2000**, *34*, 9.
(13) Xiang B.; Kevan, L. *Langmuir* **1994**, *10*, 2688.
(14) Xiang B.; Kevan, L. *Langmuir* **1995**, *11*, 860.
(15) Alkaitis, S. A.; Beck, G.; Grätzel, M. *J Am. Chem. Soc*. **1975**, *97*, 5723.
(16) Moroi, Y.; Braun, A. M.; Grätzel, M. *J. Am. Chem. Soc*. **1979**, *101*, 567.
(17) Krishna, R. M.; Kurshew, V.; Kevan, L. *Phys. Chem. Chem. Phys*. **1999**, *1*, 2833.
(18) Hartmann, M.; Kevan, L. *Chem. Rev*. **1999**, *99*, 635.
(19) Zahedi-Niaki, M. H.; Joshi, P. N.; Kaliaguine, S. Studies in Surface Science and Catalysis. In *Progress in Zeolite and Microporous Materials*; Chon, H., Ihm, S.-K, Uh, Y. S., Eds.; Elsevier: Amsterdam, 1997; Vol. 105, p 1013.
(20) Concepcion, P.; Blasco, T.; Lopez Nieto, J. M.; Perez-Pariente, J. *J. Catal*. **1995**, *152*, 1.
(21) Lok, B. M.; Messina, C. A.; Patton, R. L.; Gajek, R. T.; Cannan, T. R.; Flanigen, E. M. U.S. Patent 4,440,871, 1984.
(22) Tapp, N. J.; Milestone, N. B.; Bibby, D. M. *Zeolites* **1998**, *8*, 183.
(23) Hassan, Z. M.; Joshi, P. N.; Kaliaguine, S. *Acta Cryst*. **1998**, *B44*, 367.
(24) Thomas, J. M.; Greaves, G. N. *Science* **1994**, *265*, 1675.
(25) Notari, B. *Adv. Catal*. **1996**, *41*, 258.
(26) Prakash, A. M.; Kevan, L.; Zahedi-Niaki, M. H.; Kaliaguine, S. *J. Phys. Chem. B* **1999**, *103*, 831.
(27) Ulagappan, N.; Krishnasamy, V. *J. Chem. Soc., Chem. Commun*. **1995**, 373.
(28) Zahedi-Niaki, M. H.; Kapoor, M. P.; Kaliaguine, S. *J. Catal*. **1988**, *177*, 231.
(29) Centi, G.; Perathoner, S.; Trifiro, F.; Aboukais, A.; Aissi, C. F.; Guelton, M. *J. Phys. Chem.* **1992**, *96*, 2617.
(30) Minchev, C.; Minkov, C.; Penchev, V.; Weda, H.; Lechert, H. *J. Therm. Anal*. **1991**, *37*, 171.
(31) Lischke, G.; Hanke, W.; Jerschkewitz, H. G.; Ohlmann, G. *J. Catal*. **1985**, *91*, 54.
(32) Jhung, S. H.; Uh, Y. S.; Chon, H. *Appl. Catal*. **1990**, *62*, 61.
(33) Singh, P. S.; Bandyopadhyay, R.; Shaikh, R. A.; Rao, B. S. Studies in Surface Science and Catalysis. In *Zeolites: A Refined Tool for Designing Catalytic Sites*; Bonneviot, L., Kaliaguine, S., Eds.; Elsevier: Amsterdam, 1995; Vol. 105, p 343.
(34) Lok, B. M.; Messina, C. A.; Patton, R. L.; Gajek, R. T.; Cannan, T. R.; Flanigen, E. M. *J. Am. Chem. Soc*. **1984**, *106*, 6092.
(35) Messina, C. A.; Lok, B. M.; Flanigen, E. M. U.S. Patent 4,554,-143, 1985.
(36) Prakash, A. M.; Kevan, L. *J. Phys. Chem. B*. **1999**, *103*, 2214.
(37) Massie, S. P. *Chem. Rev*. **1954**, *54*, 797.
(38) Shida, D. B.; Thompson, D. R.; Veneziani, C. *J. Heterocycl. Chem*. **1967**, *4*, 517.
(39) Ortiz, A.; Gonzalez, A.; Fernandez-Alonso, J. I. *J. Solid State Chem*. **1981**, *40*, 210.
(40) Blasco, T.; Corma, A.; Navaro, M. T.; Pere-pariente, J. *J. Catal*. **1995**, *156*, 65.
(41) Tuel, A.; Ben Tarit, Y. *Appl. Catal. A* **1993**, *102*, 69.
(42) Huybrechts, D. R. C.; Buskends, P. L.; Jacobs, P. A. *J. Mol. Catal*. **1985**, *31*, 355.
(43) Krishna, R. M.; Prakash A. M.; Kevan, L. *J. Phys. Chem. B* **2000**, *104*, 0000.